Journal of Integrative Neuroscience

J. Integr. Neurosci. **2026**; 25(1): 46448
https://doi.org/10.31083/JIN46448

Original Research

Electroacupuncture Modulation of Chondroitin Sulfate Glycosaminoglycan Promotes the Repair of Damaged Spinal Cord in Rats

Bowen Chen[1,†], Rong Hu[1,†], Xingying Wu[1], Mengting Shi[1], Yi Chen[1], Jieqi Zhang[1], Yi Huang[1], Xihan Ying[1], Dexiong Han[1,2,*], Ruijie Ma[1,2,*]

[1]The Third School of Clinical Medicine (School of Rehabilitation Medicine), Zhejiang Chinese Medical University, Key Laboratory of Acupuncture and Neurology of Zhejiang Province, 310053 Hangzhou, Zhejiang, China
[2]Department of Acupuncture and Moxibustion, Third Affiliated Hospital of Zhejiang Chinese Medical University, 310009 Hangzhou, Zhejiang, China
*Correspondence: 20105015@zcmu.edu.cn (Dexiong Han); maria7878@sina.com (Ruijie Ma)
[†]These authors contributed equally.

Academic Editors: Nuno A. Silva and Bettina Platt
Submitted: 9 September 2025 Revised: 22 November 2025 Accepted: 26 November 2025 Published: 22 January 2026

Abstract

Background: The perineuronal net (PNN) is an important extracellular environment around parvalbumin interneuron (PV IN) in the spinal cord. Chondroitin sulfate proteoglycan (CSPG) serves as a key factor mediating PNN effects on the spinal cord, primarily formed by covalently linked chondroitin sulfate glycosaminoglycan (CS-GAG) chains and diverse core proteins. Extensive research suggests that degradation of CS-GAG following nerve injury may contribute to severe spinal cord damage. Inhibiting CS-GAG degradation could enhance PNN stability and plasticity, thereby promoting recovery from nerve injury. Electroacupuncture (EA) intervention demonstrates significant neuroprotective effects, facilitating restoration of spinal cord nerve function and axonal regeneration. This study aims to observe the changes in CS-GAG and the expression of PV IN after spinal cord injury (SCI) in rats and explore the effect. **Methods**: An SCI model was established in Sprague–Dawley rats using an Infinite Horizon (IH) impactor, and EA was applied to the Jia-ji acupoints (EX-B2). The Basso–Beattie–Bresnahan (BBB) score of SCI rats was evaluated, and electromyography (EMG) of the gastrocnemius muscle of the hind limbs was performed. The protein expression levels of CS-GAG and glutamic acid decarboxylase (GAD) were detected using western blotting, and perineuronal nets (PNN) and PV IN were observed using immunofluorescence (IF). Fiber-optic calcium imaging was used to detect and analyze PV IN activity. Adeno-associated virus containing carbohydrate sulfotransferase 11 (Chst11) was injected into T9 and T10 spinal cord spaces using a microneedle, and changes in CS-GAG in the spinal cord of SCI rats before and after EA intervention were observed. **Results**: CS-GAG and GAD expression levels were significantly decreased after SCI and PNN stability was reduced. Chondroitinase ABC (ChABC) treatment increased PV IN activity and GAD expression. EA effectively promoted an increase in CS-GAG and GAD, improved PNN stability and PV IN activity, and reversed the inhibitory effect of Chst11, thereby facilitating the rehabilitation of rats with SCI. **Conclusion**: The mechanisms and effects of EA on SCI repair were investigated. The results revealed that EA can regulate the recovery of PNN structure and function via CS-GAG and GAD, improve PV IN activity, and reverse the inhibitory effect of Chst11 to promote SCI rehabilitation in rats.

Keywords: spinal cord injury; electroacupuncture; parvalbumin interneuron; chondroitin sulfate glycosaminoglycan; glutamic acid decarboxylase

1. Introduction

With the rapid development of the global economy and the increasingly severe aging process of the population, the incidence of spinal cord injury (SCI) remains high [1], and its disability rate has become the second leading cause of paralysis [2], placing a heavy burden on the social healthcare system. The pathological mechanisms of SCI are complex and diverse, and effective treatments for SCI are still lacking.

The perineuronal net (PNN) is an important extracellular environment around parvalbumin interneurons (PV IN) in the spinal cord [3]. It plays an important role in neuroprotection and the maintenance of neuronal plasticity and stability. PNN is a network structure within the extracellular matrix (ECM) that contains chondroitin sulfate proteoglycan (CSPG) [4]. Research has demonstrated that CSPG is an important factor in the action of PNN on the spinal cord [5], which is primarily formed by covalent bonds between chondroitin sulfate glycosaminoglycan (CS-GAG) chains and various core proteins. CS-GAG is sulfated in different ways depending on the chondroitin sulfotransferase [6,7], with two main types being chondroitin 4-sulfation (C4S) and chondroitin 6-sulfation (C6S). Carbohydrate sulfotransferase-11 (Chst11)/chondroitin-4-sulfotransferase-1 (C4ST-1), an enzyme widely distributed in the central nervous system (CNS), plays an important role in CS4-O-sulfation and the amount of CS synthesis [8].

C4ST-1 reduction accelerates neural axon regeneration in zebrafish after SCI [9]. One study has presented that the ratio of C4S/C6S reflects the development and structural stability of PNN to a certain extent [10]. Meanwhile, the C4S/C6S ratio determines maturation of PV IN and regulates the plasticity of PNN [10]. One study has demonstrated that the absence of CS reduces the spike reaction of PV IN wrapped in PNN [11], and the maturation of PV IN promotes the development of PNN and the sulfation mode of CS-GAG [11]. Research suggests that the negative charge carried by CS-GAG plays a crucial role in maintaining the plasticity and stability of neurons, and the degradation of CS-GAG after nerve injury may cause severe damage to the spinal cord [5]. Therefore, if CS-GAG degradation is prevented, it enhances the stability and plasticity of PNN to a certain extent, allowing neuronal damage to be repaired.

Electroacupuncture (EA) at the jia-ji acupoints is a reliable and effective clinical method for safely improving the peripheral microenvironment after SCI. EA intervention has a significant neuroprotective effect [12], promoting the recovery of spinal cord nerve function and axonal regeneration [13,14]. Our previous research has confirmed that EA promotes the proliferation and differentiation of neural stem cells, oligodendrocyte precursor cells, and oligodendrocytes, improves myelin sheath formation after SCI, promotes the recovery of SCI via the upregulation of PNN by inhibition of Sema3A, and plays a vital role in promoting the recovery of motor function after SCI [13,15,16]. Current studies have focused on the regulation of PNN components by EA. Consequently, this study aimed to elucidate whether EA regulation of CS-GAG after SCI promotes the restoration of PNN stability and facilitates the repair of SCI.

2. Materials and Methods

2.1 Animals

Healthy adult male SD rats (8 weeks of age, 200–220 g) were purchased from Shanghai Sipur-Bike Laboratory Animal Co., LTD (Shanghai, China, Animal license No.: SCXK(Shanghai) 2018-0006), and were raised in Laboratory Animal Center of Zhejiang Chinese Medicine University and approved by the China Laboratory Animal Management Evaluation and Accreditation Association (AAALAC, Animal license No.: SYXK(Zhejiang) 2018-0012). The rats were kept in controlled conditions and had free access to water and food. All animal experiments were conducted in accordance with all relevant animal testing and research ethics regulations and in accordance with the animal protocol approved by the Animal Ethics Committee of Zhejiang University of Chinese Medicine (ZSLL, 2017183).

2.2 Subgroups and Interventions

A total of 144 rats were included in this study. All rats were randomly assigned to each group. (1) In the Sham group (n = 8), only the T10 vertebral plate was removed without any other intervention. (2,3,4) The SCI (n = 8), SCI-1d (n = 8) and SCI-7d (n = 8) groups were subjected to SCI model preparation without intervention. (5,6) SCI + phosphate buffer saline (PBS) (n = 8) and SCI + Chondroitinase ABC (ChABC) (Sigma-Aldrich, C3667, St. Louis, MO, USA) (n = 8) groups received 14 days of PBS and ChABC injections, respectively, based on the SCI model preparation. (7,8) After preparing the SCI model, the SCI + ShamEA (n = 8) (sham acupuncture control group, with needles hung off the skin without other interventions) and SCI + EA (n = 8) groups received acupuncture without electrical stimulation and acupuncture with electrical stimulation interventions for 14 days, starting on the second day. (9,10) SCI + Vehicle (Veh) (n = 8) and SCI + Chst11 (n = 8) groups were injected with empty vector control virus and Chst11 overexpression virus, respectively, and SCI models were prepared. (11) The SCI + Chst11 + EA (n = 8) group was added to the SCI + Chst11 group and included a 14-day EA intervention. The above section comprises a total of 88 rats, divided into 11 groups. Due to the unique nature of qRT-PCR experiments, this section is designated separately, involving a total of 56 rats. Groups included: Sham (n = 8), SCI (n = 8), SCI + PBS (n = 8), SCI + ChABC (n = 8), SCI + Veh (n = 8), SCI + Chst11 (n = 8), and SCI + Chst11 + EA (n = 8).

2.3 Injection of ChABC or PBS

Dissolve ChABC or PBS in 1% fetal bovine serum (Sigma-Aldrich, F0193) to prepare a solution at a concentration of 5 U/mL [17]. Prepare fresh daily. Starting from day 1 after SCI model establishment, deliver ChABC or PBS to the rat's spinal cord via intrathecal injection for 14 days [18].

2.4 Animal Mortality and Dropout Records

Animal deaths and experimental dropouts inevitably occurred during this study, and this section provides an explanation. (1) Two rats in the Sham group died from postoperative infection complications. A rat sustained an accidental injury to its right hind limb during electromyography (EMG) amplitude measurement, which was not recorded. (2) One rat in the SCI group died from infection caused by bladder rupture during assisted urination due to excessive residual urine postoperatively. Additionally, one rat was lost during calcium imaging due to fiber optic detachment. (3) Two rats in the SCI + PBS group died from postoperative complications and bladder rupture. One rat was not recorded during calcium imaging due to fiber detachment. (4) Two rats in the SCI + ChABC group died from postoperative complications. Two rats were not recorded during calcium imaging due to fiber detachment. (5) In the SCI + ShamEA group, one rat failed to obtain amplitude measurements during EMG recording due to accidental injury to the right hindlimb muscles. (6) One rat in the SCI

+ EA group died from infection induced by postoperative bladder rupture. One rat failed to obtain amplitude measurements during EMG recording due to accidental injury to the right hindlimb muscles. (7) In the SCI + Veh, SCI + Chst11, and SCI + Chst11 + EA groups, two rats each (six total) died from bladder rupture during postoperative assisted urination. Among these, one rat in the SCI + Veh group could not be measured during qRT-PCR due to technical error. Due to technical errors, one rat each in the SCI + Chst11 and SCI + Chst11 + EA groups failed to yield data for the *Chst11* gene loading lane, resulting in one dropout per group (total of 2). All animals removed from the groups were euthanized (Painless euthanasia was performed by administering 100–200 mg/kg of pentobarbital sodium solution via intraperitoneal injection to induce respiratory arrest in rats.) and promptly transported to the animal center for disposal by designated personnel.

2.5 Preparation of the Rat SCI Model

Healthy adult male SD rats were deeply anesthetized with 3% pentobarbital sodium solution (Sigma-Aldrich, P3761) (2 mL/kg) and placed on a constant temperature operating table at 37 °C. The T10 cone was exposed, and the lamina was removed to expose the T10 spinal cord. An acute SCI model was created by impinging on the T10 spinal cord with a force of 200 kDynes using the IH Impactor 0400 SCI Impinger (Precision Systems and Instrumentation, LLC, IH-400, Lexington, KY, USA). The following signs indicated the successful modeling: (1) body spasmodic tremor, (2) spasmodic movement of the tail, and (3) intradural congestion or hematoma. The Basso–Beattie–Bresnahan (BBB) score was assessed on the day after modeling. Rats with scores $\geq$3 were excluded and supplemented under the same conditions. Postoperative treatment of rats that met the requirements of the acute SCI model included the following: (1) penicillin (North China Pharmaceutical Co., Ltd, 52123, Hebei, China) (100 U/d) was injected into the abdominal cavity for anti-infection for three consecutive days; (2) the room temperature was maintained at 20–25 °C; (3) the bladder was massaged twice a day until it appeared to urinate autonomously.

2.6 EA Therapy

The EA was administered at the T9–T11 Jia-ji acupoints (EX-B2), located beside the spinous processes on the back, starting on the first day after surgery. The procedure was as follows: a disposable sterile stainless steel acupuncture needle (0.18 mm in diameter; Beijing Zhongyantaihe Medical Instrument Co., Ltd., V518215, Beijing, China) was inserted 1.5 mm lateral to the midline of the spinous process to a depth of 4–5 mm, until the needle tip contacted the lamina, and connected to the HANS200A electroacupuncture instrument (Nanjing Jisheng Medical Technology Co., Ltd., HANS200A, Nanjing, China). The parameters were set as follows: frequency, 2/100 Hz; current intensity, 1 mA; once daily for 20 min. The EA treatment period was 14 days.

2.7 Behavioral Test

As previously described [19], the BBB hind limb movement test was scored on a scale of 0–21 (0 = no visible hind limb movement; 21 = normal movement). Hind limb movement of rats with SCI was tested in an open field, including hind limb joint movement, weight support, footstep, coordination, paw position, fine paw movement, and trunk and tail control. BBB testing was performed on the first day after establishing the model. Each rat was placed in an open field and evaluated by two experimenters who were unaware of the experimental group for 3 min. One of the experimenters recorded the scores, and all rats were evaluated before establishing the SCI model to ensure baseline differences. Each score was averaged to obtain the final score. For specific scoring criteria, refer to Table 1.

2.8 Adeno-Associated Viruses (AAV) Stereotactic Injection

The rats were bilaterally injected into the spinal cord with 500 nL of rAAV-CMV-Chst11-Flag-WPREs, AAV2/9 (BrainVTA Co., Ltd., PT-0634, Wuhan, China); a negative control rAAV-CMV-Flag-WPREs, AAV2/9 (BrainVTA Co., Ltd., PT-0634); or a combination of rAAV-CAG-FLEX-jGCaMP7f-WPRE-SV40pa, AAV2/9 (BrainVTA Co., Ltd., PT-1422) and rAAV-PV-CRE-bGHpa, AAV2/9 (BrainVTA Co., Ltd., PT-0275). The procedure was as follows: after exposing the spinal cord by removing the skin and connective tissue between the T9 and T10 vertebral plates with forceps, the virus was injected into the spinal cord under a microscope. Using the spinal vessels along the midline as anatomical landmarks, the injection site was positioned 1 mm lateral and 0.3 mm from the median vessels, with the needle inserted at a 10° angle. After injection, the needle tip was left in the spinal cord for 5 min to prevent viral backflow. The injection was performed at a final titer of 5.00×10^{12} vg/mL, with a flow rate of 100 nL/min and a total volume of approximately 500 nL bilaterally, avoiding blood vessels and nerves.

2.9 Immunofluorescence (IF)

The rats (n = 3 per group) were euthanized with 3% pentobarbital (Sigma-Aldrich, P3761) (100–200 mg/kg), followed by transmyocardial perfusion with saline, and the T10 segmental spinal cord was obtained, and immersed the spinal cord in a 4% paraformaldehyde solution (Sigma-Aldrich, 16005). The T10 spinal cord was cut into 12-µm-thick transverse sections using a Frozen Slicer (Thermo Scientific CryoStar™ NX70, 957010K, Thermo Fisher Scientific, Waltham, MA, USA), with each rat containing at least five consecutive sections. All slides were closed for 1 h at 37 °C in a water bath with TBST containing 10% normal goat serum, followed by overnight incubation at 4 °C with

Table 1. Basso-Beattie-Bresnahan locomotor rating score.

Score	The ability of Lower limb motor
0	There is no visible hindlimb (HL) movement
1	Light movement of one or both joints, usually hip and/or knee
2	Broad movement of one joint or joint and slight movement of the other
3	Extensive movement of the two joints
4	Light movement of three joints
5	Light movement of two joints and wide movement of the third
6	Broad movement of the two joints and light movement of the third
7	The extensive movement of all three joints of HL
8	The ball of the foot without weight support or without weight support
9	The soles of the feet occasionally bear the weight of the ground (for example, when stationary), frequent or consistent load-bearing movements of the dorsal claw, without the soles of the feet supporting the movement
10	Paw surface occasionally moves with load bearing without Forelimb-hindlimb (FL-HL) coordination
11	Paw surface has more load bearing movement and no FL-HL coordination
12	More load bearing movement and occasional FL-HL coordination on paw surface
13	Common paw bearing movement and frequent FL-HL coordination
14	Continuous palm-surface bearing movement with consistent FL-HL coordination, or common palm-surface movement, continuous fore-hind limb coordination, and occasionally dorsal claw movement
15	Continuous paw and palm bearing movement and consistent FL-HL coordination, no or occasional ground grasping movement in the forward motion of the forelimbs, and the position of the main claw parallel to the body at the initial contact
16	In the gait, the continuous paw landing and the coordinated movement of the front and rear limbs are common in the process of grasping the ground. The main claw position is parallel to the body at initial contact, and rotates after load transfer
17	In the gait, the continuous paw landing and the coordinated movement of the front and rear limbs are common in the process of grasping the ground. The main claw position is parallel to the body at initial contact and load transfer
18	In the gait, the continuous paw touches the ground in a coordinated manner with the front and rear limbs. In the process of progress, the continuous paw grasps the ground. The position of the main paw is parallel to the body at the initial contact
19	In the gait, the continuous paw touches the ground in a coordinated manner with the front and rear limbs. The continuous paw grasps the ground in the process of advancing. The position of the main paw is parallel to the body at the initial contact and load transfer
20	The position of the main claw is parallel to the body during initial contact and weight transfer. The trunk is unstable and the tail kept cocking up
21	The position of the main claw is parallel to the body at the initial contact and load transfer, and the trunk is stable and the tail kept cocking up

the primary antibody. Rabbit monoclonal anti-parvalbumin antibody (1:100, ab181086, Abcam, Cambridge, UK) and wisteria floribunda lectin (WFA) (1:100, B-1355-2, Vector Laboratories, Newark, California, USA) were used for incubation. The next day, the slices were rinsed with tris-buffered saline with tween-20 (TBST) and reacted with the corresponding secondary antibody mixture (1:200, Alexa Fluor® 555 Streptavidin Coupler and 1:300, Alexa Fluor® 488 Goat anti-rabbit IgG, Thermo Fisher Scientific). Fluorescence images were obtained using a Zeiss structured illuminated optical slice microscope (Axio Imager M2; Zeiss AG, Jena, Germany). All stained sections were observed and analyzed using a blinded method. Non-experimental personnel counted and statistically analyzed the number of cells in each section using Adobe Photoshop 13.0 (Adobe Systems, 13.0, San Jose, CA, USA).

2.10 Western Blotting (WB)

Rats were euthanized with 3% pentobarbital (Sigma-Aldrich, P3761) (100–200 mg/kg), followed by transmyocardial perfusion with saline, and the T10 segmental spinal cord was obtained. On day 14 after SCI model preparation, rats were euthanized, and the T10 segmental spinal cord was rapidly removed. According to the manufacturer's instructions, bicinchoninic acid assay (BCA; Pierce ™ BCA, 23227, Thermo Fisher Scientific) was used for protein concentration determination, with 20 mg protein per lane. To detect CS protein content, 5 U/mL of ChABC was added to the protein supernatant and incubated in a shaking bed at 37 °C for 8 h. Protein samples were separated on a 4%–15% SDS-polyacrylamide gel electrophoresis (SDS-PAGE) gel and electrophoretically transferred to a polyvinylidene fluoride (PVDF) membrane (Merck Millipore, Inc., IPVH00010, Billerica, MA, USA). The membrane was closed with 5% skim milk (Becton, Dickinson and Company, 232100, Franklin Lakes, NJ,

Table 2. Primer sequences for qRT-PCR.

Primers	Forward	Reverse	Amplicon size (bp)
Chst11	GTA CGA GAC GCT GGA GGA GGA C	CGG TAG TTC GGG TGG ACT TTG C	120
Chst3	CCT CGG AGC AGT TTG AGA AGT GG	ATG ATG GAG CGG TTG GTG AGT G	129

qRT-PCR, quantitative real-time polymerase chain reaction; Chst, carbohydrate sulfotransferase.

USA) at room temperature for 1 h, and then incubated overnight at 4 °C in a diluted primary antibody in a closed buffer: β-actin (1:5000, Ms mAb to β-actin, Abcam), C4S (1:2000, mouse Anti-Chondroitin-4-Sulfate, MAB2030, Merck), C6S (1:2000, mouse Anti-Chondroitin-6-Sulfate, MAB2035, Merck), glutamic acid decarboxylase(GAD)65 and GAD67 (1:2000, Rb mAb to GAD65 + GAD67, ab183999, Abcam). The next day, the membrane was incubated with secondary antibodies (1:2000, goat anti-mouse, BK-M050, BIOKER, Hangzhou, China and 1:2000, goat anti-rabbit, 7074s, Cell Signaling Technology, Danvers, MA, USA) at room temperature for 2 h. Immunoreactivity was detected using enhanced chemiluminescence and visualized using an Image Quant LAS 4000 (Cytiva, LAS4000, Tokyo, Japan).

2.11 Quantitative Real-Time Polymerase Chain Reaction (qRT-PCR)

The rats were euthanized with 3% pentobarbital (100–200 mg/kg), followed by trans-myocardial perfusion with saline. Then, the T10 segmental spinal cord was obtained. A 0.5 cm segment of spinal cord tissue was placed in TRIzol reagent (Invitrogen, 15596018CN, Thermo Fisher Scientific) to extract total RNA. The extracted total RNA was reverse-transcribed using a transcription kit (Takara Biomedical Technology (Beijing) Co., Ltd., RR047A, Beijing, China) according to the manufacturer's protocol. The target gene was mixed with SYBR Green (Solarbio, MQ10101S, Monad Biotech Co., Ltd., Beijing, China) reagent, and qRT-PCR was performed using LightCycler® 480 Instrument II (Roche, 05015243001, Basel, Switzerland). Gene expression was calculated using the $2^{-\Delta\Delta CT}$ method, and the final data were normalized to β-actin levels. The primer sequences are presented in Table 2.

2.12 Fiber Optic Calcium Imaging

Four weeks prior to modeling, rAAV-CAG-FLEX-jGCaMP7f-WPRE-SV40pa virus was bilaterally injected into the T9-T10 spinal cord junction using a Hamilton (Hamilton, 202630, Bonaduz, Switzerland) syringe. The injection flow rate was 100 nL/min, with a total injection volume of approximately 500 nL. The viral delivery sites and transfection coverage are shown in **Supplementary Fig. 1**. Immediately after successful model establishment, proceed with fiber implantation following these steps: The T10 spinal cord segment was fully exposed, and a 0.01 mm-thick perforated titanium plate (Xi'an Saite Metal Materials Development Co., Ltd., Xi'an, China) was placed on the spinal cord. The plate was secured to the surrounding soft tissue and vertebral body using non-absorbable surgical sutures at the four corners. All procedures were performed using a microscope. A fiber-optic probe (200 µm in diameter and 2 mm in length, Thinker Tech Nanjing Bioscience Inc, Nanjing, Jiangsu, China), mounted on a stereotaxic instrument (RWD, 68804, RWD Life Science, Shenzhen, China) with a fiber-optic holder, was positioned adjacent to the central canal of the spinal gray matter and inserted to a depth of 1.5 mm. The assembly was secured with dental cement (Shanghai New Century Dental Materials Co., Ltd., 20173170702, Shanghai, China) and adhesive (Single Bond Universal, 3 M ESPE, St. Paul, MN, USA) and covered with toner (Macklin, C805116, Shanghai, China) to prevent light interference. GCaMP7f fluorescence was excited at two wavelengths: 470 nm for the calcium-dependent signal and 405 nm for the baseline signal. The amplitude-modulated excitation light was reflected by a dichroic mirror and coupled to an optical fiber, enabling carrier wave fiber calcium imaging photometric recording. The recorded data were imported into MATLAB (MathWorks, R2018a, Natick, MA, USA) for analysis. Calcium activity was recorded from the first 2 s of the external stimulus to 10 s after the stimulus to capture changes in calcium signaling shortly after sensory induction (by pinching the foot).

2.13 Electromyography (EMG)

Nicolet EDX: Viking QUEST equipment (Nicolet EDX: Viking QUEST, Natus Neurology, Madison, WI, USA) was used to acquire EMG data from the right lower limb gastrocnemius muscle of rats. The rats were placed on a special rat sleeve, and the hair of the gastrocnemius muscle was shaved using a hair-shaving machine. The rats were tested in an emotionally calm state. During detection, recording electrodes were inserted into the gastrocnemius muscle of the right lower limb of the rats, and EMG signals with a frequency range of 20–500 Hz were collected 20–25 times consecutively. The gastrocnemius potential was detected using the VikingSelect experimental system (Nicolet EDX: Viking QUEST, Viking QUEST v20.1.11, CA, USA), and the amplitude and duration were recorded to obtain average values.

2.14 Statistical Analysis

All data were analyzed, and graphs were generated using GraphPad software (GraphPad, v8.0.2, San Diego, CA, USA) or MATLAB. The normality of the continuous

variables was assessed using the Shapiro–Wilk test. For data conforming to a normal distribution, Student's *t*-test (two-tailed) was used for comparisons between two groups, while one-way analysis of variance (ANOVA) was used for comparisons among multiple groups, followed by Tukey's post hoc test. For data that did not follow a normal distribution, the Mann–Whitney U test and the Kruskal–Wallis H test were applied for comparisons between two groups and among multiple groups, respectively. A two-way ANOVA was performed to analyze BBB scores across groups. When an interaction between group (intervention) and time was observed, simple effects analysis was conducted and adjusted using Tukey's post-hoc test. When no interaction between group (intervention) and time was observed, main effects analysis was performed followed by Tukey's post-hoc test. All results are expressed as mean ± standard error of the mean (SEM). A $p < 0.05$ was considered statistically significant.

3. Results

3.1 CS-GAG and GAD Expression Levels Were Significantly Reduced After SCI

We performed WB to detect CS, which is essential for the composition and function of the PNN, and its corresponding sulfated forms (C4S and C6S) (Fig. 1B,C). The results revealed that the expression levels of C4S and C6S in the spinal cord after SCI decreased on SCI-7d and increased on SCI-14d compared to the control group (Sham group) (Fig. 1B,C). The protein expression level of GAD can indirectly reflect the expression level of PV IN to a certain extent [20]. We examined the protein levels of both GAD isoforms after SCI (Fig. 1D). Both protein expressions were significantly reduced on SCI-7d, and GAD67 expression levels increased slightly on SCI-14d as the rat spinal cord repaired itself (Fig. 1E,F). Simultaneously, we analyzed the C4S/C6S ratio, and the results are presented in Fig. 1A. After SCI, this ratio began to decrease gradually, reaching its lowest point on SCI-7d. Subsequently, it began to increase slowly over time, becoming higher than that on SCI-1d by SCI-14d, although it remained lower than that in the control group.

3.2 ChABC Promotes PNN Stability After SCI and Facilitates Motor Function Repair in Rats

To investigate the changes in PNN during SCI repair, we administered ChABC to the T10 region for 14 days. The results of the BBB scores revealed a significant interaction between group (intervention) and time ($F_{(9,84)} = 192.6$, $p < 0.0001$). Analysis of main effects showed that group (intervention) significantly influenced BBB scores ($F_{(3,84)} = 1544$, $p < 0.0001$). On day 14, the SCI + ChABC group scored significantly higher than the SCI + PBS group ($p < 0.0001$). The main effects analysis also revealed a significant effect of time on BBB scores ($F_{(3,84)} = 1706$, $p < 0.0001$). The SCI + ChABC group exhibited higher BBB scores on day 14 than on day 7 ($p < 0.0001$). The BBB scores revealed that the motor function of the rats significantly improved after ChABC intervention (Fig. 2A). EMG results indicated that ChABC improved the SCI status, along with significant improvement in both EMG and muscle condition of the hind limbs of the rats (Fig. 2B–F). Meanwhile, WB analysis revealed that following ChABC administration, C4S and C6S protein expression was significantly elevated in the spinal cords of SCI + ChABC group rats, approaching CS expression levels observed in the normal rat spinal cord (Fig. 2G–I). After ChABC intervention, the C4S/C6S ratio was significantly higher in the SCI + ChABC group than in the remaining three groups on day 14, and a significant difference was observed between SCI + ChABC and SCI + PBS control groups (Fig. 2G), indicating improved PNN stability. The qRT-PCR results exhibited no significant alterations in the gene expression of the synthases synthesizing the different sulfated forms of CS (Fig. 2J,K), suggesting that ChABC intervention did not affect the gene expression profile of the relevant synthases.

3.3 ChABC Enhances PV IN Activity After SCI

Changes in CS are closely related to the progression of SCI repair, and the ratio of C4S to C6S affects PNN structure stability after SCI. Changes in CS affect the activity and expression of PV IN. We injected AAV indicative of changes in calcium signaling and labeled PV IN in the spinal cord of rats at the junction of T9 and T10. We detected and recorded calcium signals on day 14 after preparing the SCI model (Fig. 3A,B). Our previous study confirmed that neurons labeled by the jGCamp7f virus are PV IN, and the virus co-infects with PV [21]. We also validated the virus in rats and demonstrated that jGCaMP7f binds to PV IN with a significant effect (**Supplementary Fig. 1**). After ensuring that the surroundings were quiet and suitable and that the rats were emotionally stable, we recorded calcium signals from 2 s before stimulation to 10 s after stimulation. The results (Fig. 3C,D) revealed that the amplitude of calcium signaling in PV IN was significantly reduced in the SCI group than in the control group (Fig. 3E), and the peak calcium signal during neuronal activity decreased (Fig. 3F). The amplitude of calcium signaling in PV IN at the injury site was significantly increased in SCI + ChABC than in SCI + PBS (Fig. 3E), with no significant increase in the peak of calcium signal (Fig. 3F). WB results (Fig. 3G) revealed that the GAD67 expression level was significantly increased in the SCI + ChABC group than in the SCI + PBS control group, with no significant difference in GAD65 expression among the groups (Fig. 3H,I).

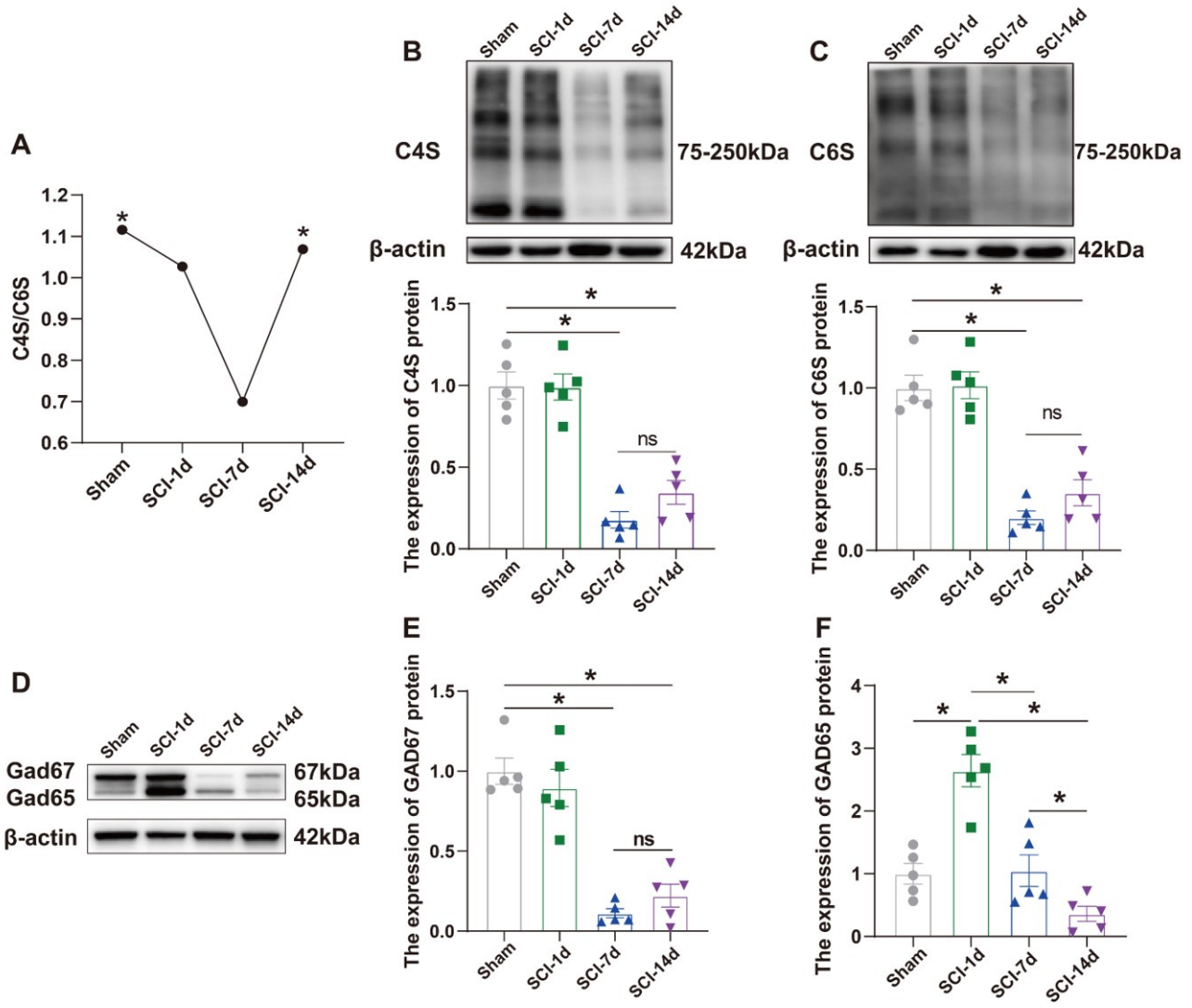

Fig. 1. The protein expression of CS and GAD was reduced following SCI. (A) Changes in the C4S/C6S ratio in normal rats at SCI-1d, SCI-7d, and SCI-14d (n = 4, F = 5.225, $p = 0.0174$). (B) Confirmation of two-dimensional gel electrophoresis results by WB. Analysis of C4S protein levels in normal rats at SCI-1d, SCI-7d, and SCI-14d, using β-actin as an internal control (n = 5, F = 34.73, $p < 0.0001$). (C) Confirmation of two-dimensional gel electrophoresis results by WB. Analysis of C6S protein levels in normal rats at SCI-1d, SCI-7d, and SCI-14d, using β-actin as an internal control (n = 5, F = 34.37, $p < 0.0001$). (D) Two-dimensional gel electrophoresis results for GAD67 and GAD65 in WB. (E) Confirmation of two-dimensional gel electrophoresis results by WB. Analysis of GAD67 protein levels in normal rats at SCI-1d, SCI-7d, and SCI-14d, using β-actin as an internal control (n = 5, F = 31.68, $p < 0.0001$). (F) Confirmation of two-dimensional gel electrophoresis results by WB. Analysis of GAD65 protein levels in normal rats at SCI-1d, SCI-7d, and SCI-14d, using β-actin as an internal control (n = 5, F = 21.98, $p < 0.0001$). *$p < 0.05$. Data are expressed as mean $\pm$ SEM. Statistical analysis of the data results was performed using one-way ANOVA, followed by Tukey's post hoc test. CS, chondroitin sulfate; GAD, glutamic acid decarboxylase; C4S, chondroitin 4-sulfation; C6S, chondroitin 6-sulfation; SCI, spinal cord injury; WB, Western blotting; ANOVA, analysis of variance.

3.4 EA Increases the Expression Levels of CS-GAG and GAD After SCI and Promotes the Recovery of Motor Function in Rats

Previous studies have demonstrated that ChABC significantly promotes PNN stability and enhances PV IN activity. Subsequently, we used EA to intervene in SCI rats and verified its therapeutic effects to determine whether the repair effect of EA on SCI was similar to or significantly different from that of ChABC. The results of BBB scoring revealed a significant interaction between group (intervention) and time ($F_{(9,96)} = 167.9$, $p < 0.0001$). Analysis of main effects indicated that group (intervention) significantly influenced BBB scores ($F_{(3,96)} = 1323$, $p < 0.0001$). On day 14, the SCI + EA group scored significantly higher than the SCI + ShamEA group ($p = 0.0011$). The main

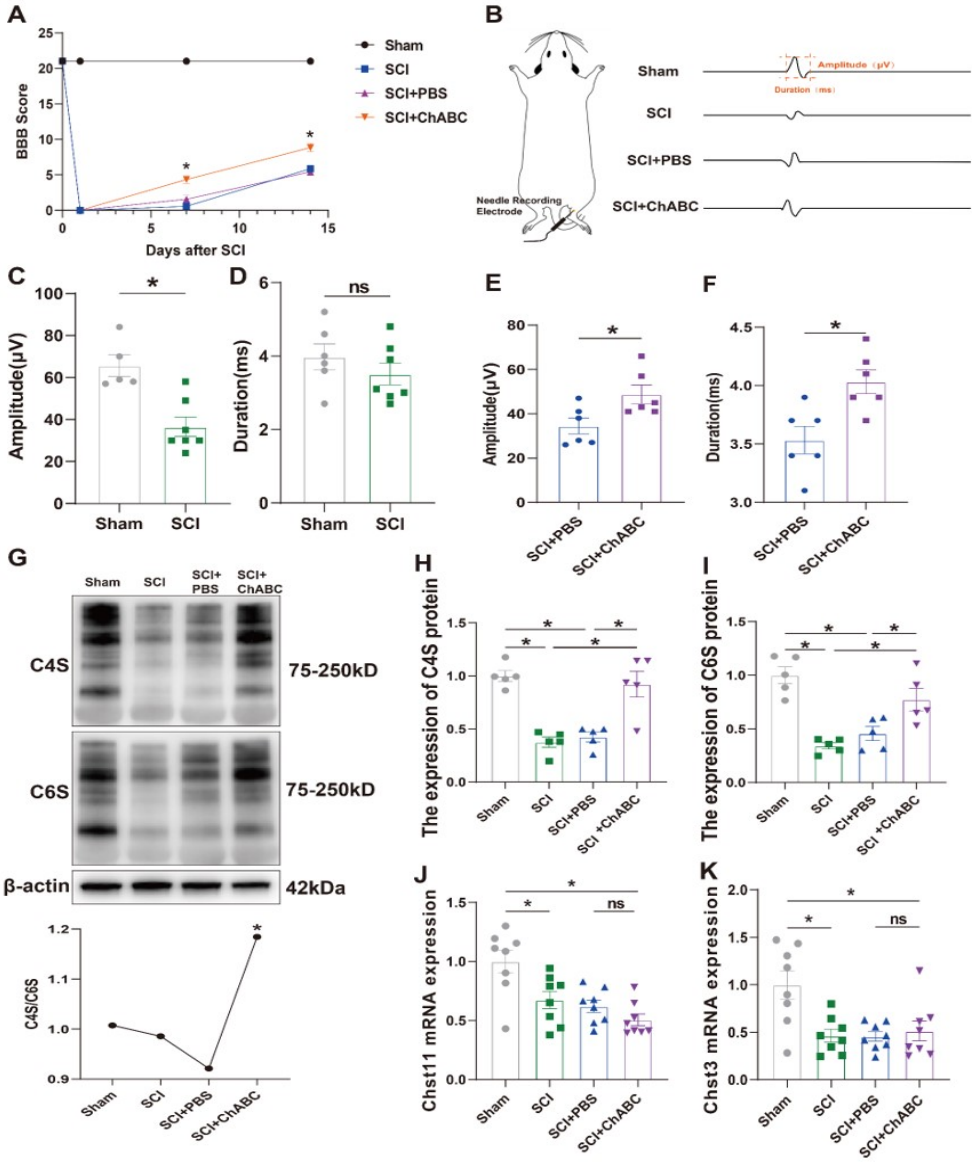

Fig. 2. ChABC increases CS protein expression after SCI and promotes motor function recovery. (A) Changes in BBB scores at 14 days post-establishment of the acute spinal cord injury model in the Sham group, SCI group, SCI + PBS group, and SCI + ChABC group (n = 6–7). There was an interaction between group (intervention) and time in the BBB scores. A two-way ANOVA was performed, followed by Tukey's post hoc test. (B) Schematic representation of EMG waveforms recorded from different groups. (C) Statistical analysis of EMG amplitude in the gastrocnemius muscle of the Sham and SCI group (n = 5–6, $t = 4.136$, $p = 0.0020$). (D) Statistical graph of EMG duration in the gastrocnemius muscle of the hind limb in the Sham and SCI group (n = 6, $t = 1.025$, $p = 0.3272$). (E) Statistical graph of EMG amplitude in the gastrocnemius muscle of the hind limb in the SCI + PBS and SCI + ChABC group (n = 6, $t = 2.596$, $p = 0.0267$). (F) Statistical graph of EMG duration in the gastrocnemius muscle of the hind limb in the SCI + PBS and SCI + ChABC group (n = 6, $t = 3.213$, $p = 0.0093$). (G) Confirmation of two-dimensional gel electrophoresis results by WB. Changes in GAD67 and GAD65 protein expression and the C4S/C6S ratio in Sham, SCI, SCI + PBS, and SCI + ChABC groups (n = 5, F = 5.321, $p = 0.0146$). (H) Analysis of C4S protein levels in Sham, SCI, SCI + PBS, and SCI + ChABC groups, using β-actin as an internal control (n = 5, F = 19.64, $p < 0.0001$). (I) Analysis of C6S protein levels in Sham, SCI, SCI + PBS, and SCI + ChABC groups using β-actin as an internal control (n = 5, F = 16.06, $p < 0.0001$). (J) Synthetase *Chst11* mRNA expression (n = 7–8, F = 8.911, $p = 0.0003$). (K) Synthetase *Chst3* mRNA expression (n = 7–8, F = 6.806, $p = 0.0014$). ns: not significant, ns: not significant, *$p < 0.05$. Data are expressed as mean ± SEM. (C), (D), (E), and (F) were analyzed using Student's *t*-test (two-tailed) to compare the two groups. (G), (H), (I), (J) and (K) were analyzed using one-way ANOVA, followed by Tukey's post hoc test. ChABC, Chondroitinase ABC; PNN, perineuronal net; BBB, Basso–Beattie–Bresnahan; EMG, electromyography; Chst11, carbohydrate sulfotransferase-11; Chst3, carbohydrate sulfotransferase-3. Fig. 2B was created using Adobe Illustrator 2019 (23.0.3 x64, Adobe Systems Incorporated, San Jose, CA, USA).

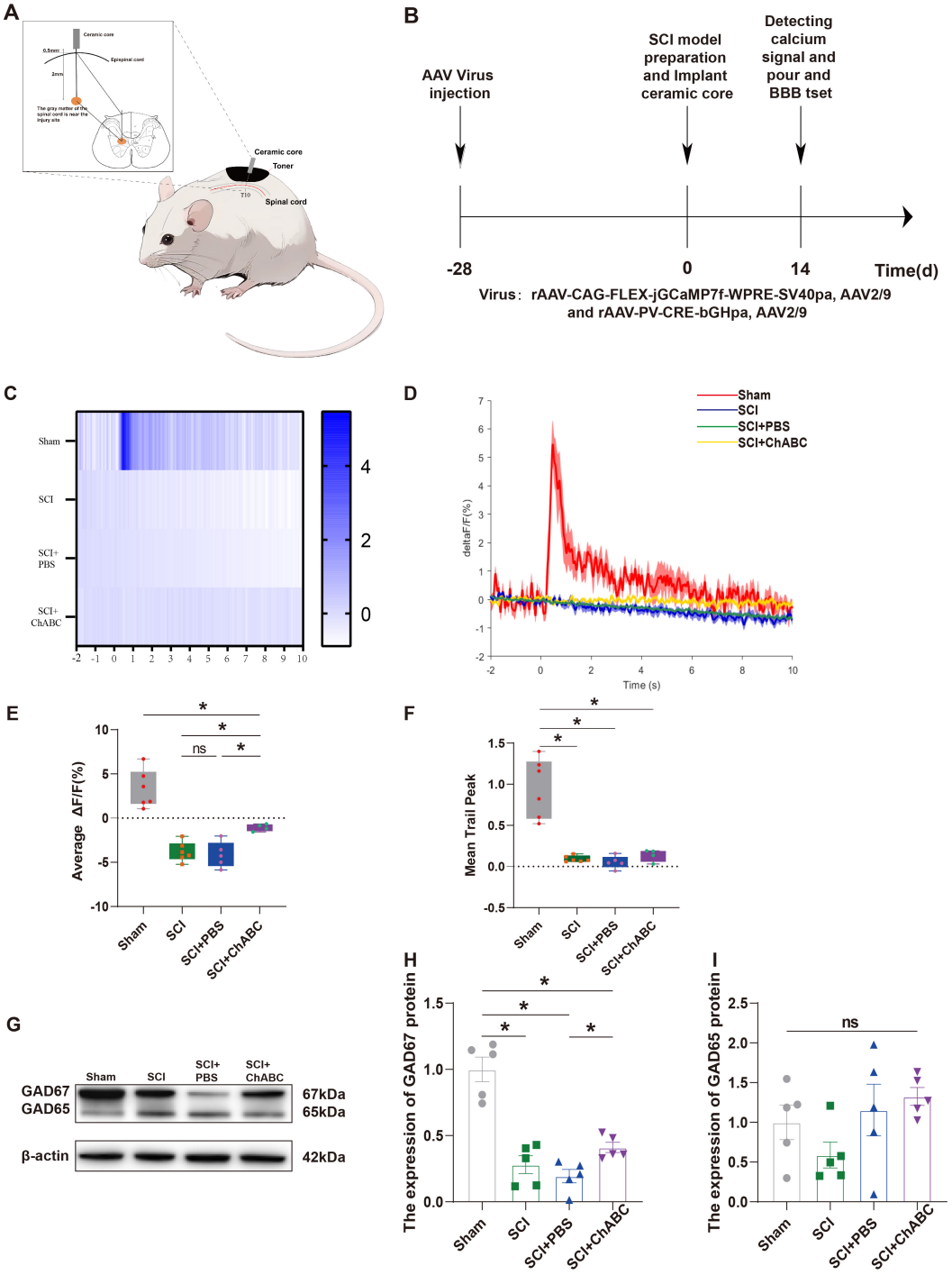

Fig. 3. ChABC enhances PV IN activity and GAD protein expression after SCI. (A) Schematic diagram of the fiber-optic placement in the rat spinal cord. (B) Schematic timeline of AAV virus injection and fiber-optic placement. (C) Heatmaps illustrating calcium signal changes in Sham, SCI, SCI + PBS, and SCI + ChABC groups recorded after excitation at 470 nm calcium-related signal wavelength. (D) Schematic diagram of folded calcium signal changes in Sham, SCI, SCI + PBS, and SCI + ChABC groups, reflecting changes in PV IN activity. (E) Statistical graph of the mean calcium signal change (n = 4–6, F = 30.53, $p < 0.0001$). (F) Comparison of calcium signal peak frequencies among the groups (n = 4–6, F = 26.21, $p < 0.0001$). (G) Changes in GAD67 and GAD65 protein expression in Sham, SCI, SCI + PBS, and SCI + ChABC groups. (H) Statistical graph of GAD67 expression (n = 5, F = 30.69, $p < 0.0001$). (I) GAD65 protein expression statistics (n = 5, F = 2.078, $p = 0.1435$). ns: not significant, *$p < 0.05$. Data are expressed as mean ± SEM. Statistical analysis of the data results was performed using one-way ANOVA, followed by Tukey's post hoc test. PV, parvalbumin; AAV, adeno-associated virus; PV IN, parvalbumin interneuron. Fig. 3A was created using Adobe Illustrator 2019 (23.0.3 x64, Adobe Systems Incorporated)

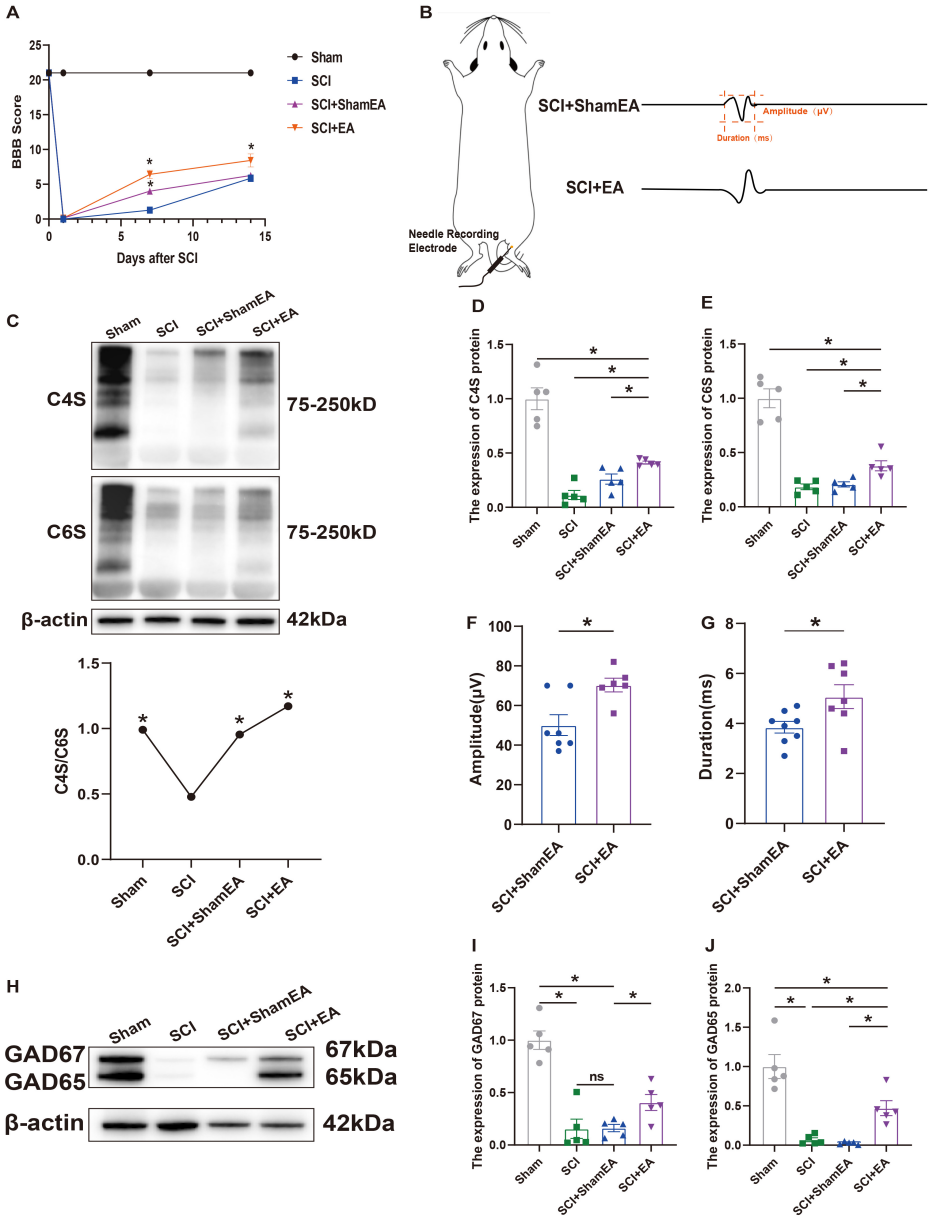

Fig. 4. EA increased the protein expression levels of CS and GAD after SCI and improved the relative stability of the PNN structure. (A) BBB motor function scores of Sham, SCI, SCI + ShamEA, and SCI + EA groups at 7 and 14 days after acute SCI model preparation (n = 7). There was an interaction between group (intervention) and time in the BBB scores. A two-way ANOVA was performed, followed by Tukey's post hoc test. (B) Schematic diagram of the waveforms of EMG signals measured in SCI + ShamEA and SCI + EA groups. (C) Protein expression of C4S and C6S and variation of C4S/C6S in Sham, SCI, SCI + ShamEA, and SCI + EA groups (n = 4, F = 9.189, $p = 0.0020$). (D,E) Confirmation of two-dimensional gel electrophoresis results by WB. Analysis of C4S and C6S protein levels in Sham, SCI, SCI + ShamEA, and SCI + EA groups, using β-actin as an internal control (C4S: n = 5, F = 41.97, $p < 0.0001$. C6S: n = 5, F = 53.71, $p < 0.0001$). (F,G) Statistical plots of amplitude versus duration after electromyographic testing of hindlimb gastrocnemius muscle in SCI + ShamEA and SCI + EA groups (Amplitude: n = 6–7, $t = 3.087$, $p = 0.0103$. Duration: n = 7–8, $t = 2.400$, $p = 0.0321$). (H) WB plots of GAD67 and GAD65 in Sham, SCI, SCI + ShamEA, and SCI + EA groups. (I,J) Confirmation of two-dimensional gel electrophoresis results by WB. Analysis of GAD67 and GAD65 protein levels in Sham, SCI, SCI + ShamEA, and SCI + EA groups, using β-actin as an internal control (n = 5, GAD67: F = 27.07, ns: not significant, $p < 0.0001$. GAD65: F = 24.81, $p < 0.0001$). *$p < 0.05$. Data are expressed as mean ± SEM. (F) and (G) were analyzed using Student's t-test (two-tailed) to compare the two groups. (C), (D), (E), (I) and (J) were analyzed using one-way ANOVA, followed by Tukey's post hoc test. EA, electroacupuncture. Fig. 4B was created using Adobe Illustrator 2019 (23.0.3 x64, Adobe Systems Incorporated)

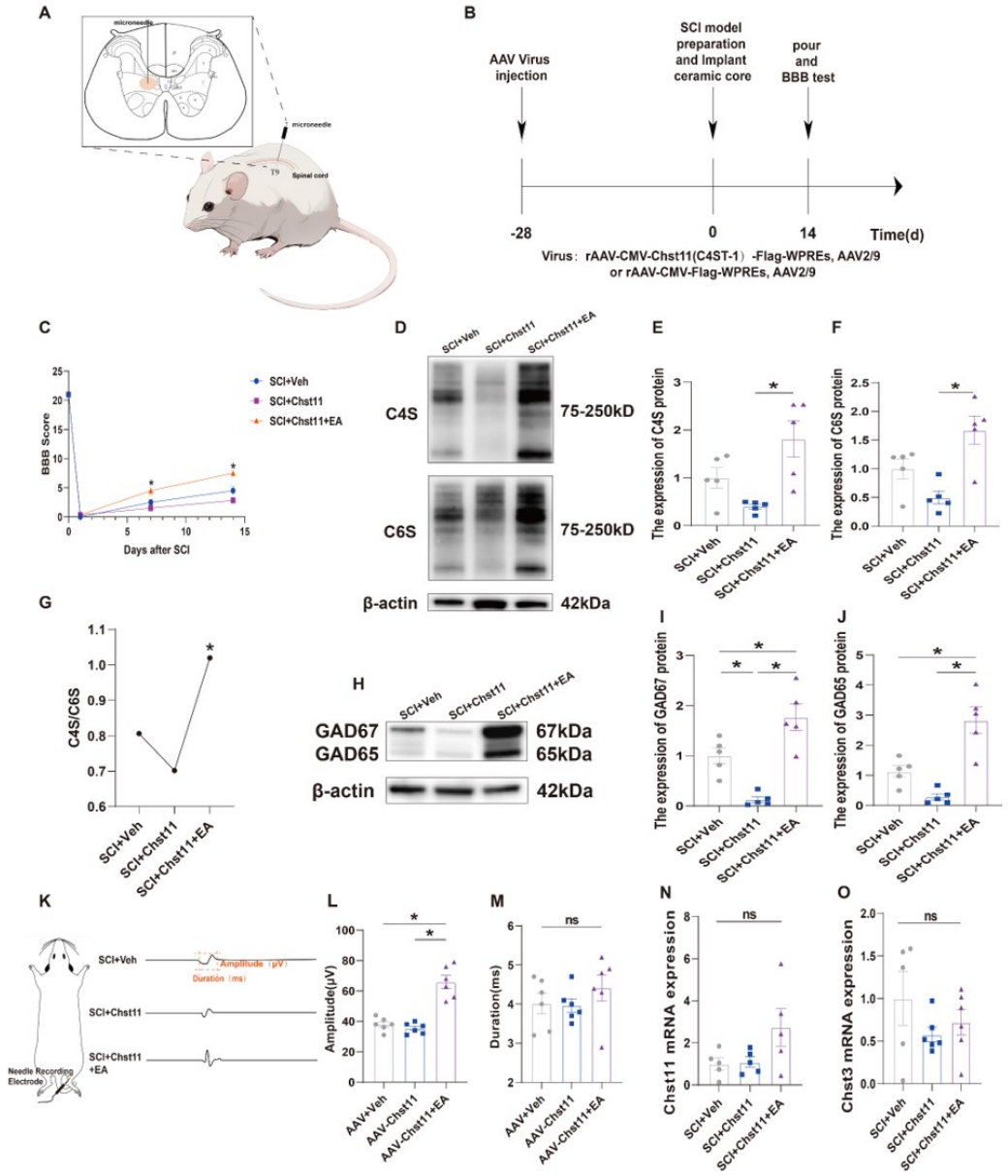

Fig. 5. EA reversed the inhibitory effect of Chst11 and increased the protein expression levels of CS and GAD. (A) Schematic diagram illustrating AAV injection. (B) Timeline of AAV virus injection and SCI model preparation. (C) Statistical graphs of BBB scores of SCI + Veh, SCI + Chst11, and SCI + Chst11 + EA groups at 7 and 14 days after SCI model preparation (n = 6). There was an interaction between group (intervention) and time in the BBB scores. A two-way ANOVA was performed, followed by Tukey's post hoc test. (D) C4S and C6S protein expression in SCI + Veh, SCI + Chst11, and SCI + Chst11 + EA groups at day 14 after SCI (n = 5). (E,F) Statistical graphs of C4S and C6S protein expression (n = 5. C4S: F = 7.805, $p = 0.0067$. C6S: F = 10.23, $p = 0.0026$). (G) Changes in the C4S/C6S ratio in SCI + Veh, SCI + Chst11, and SCI + Chst11 + EA groups (n = 4, F = 4.880, $p = 0.0367$). (H) GAD67 and GAD65 protein expression in SCI + Veh, SCI + Chst11, and SCI + Chst11 + EA groups on day 14 after SCI (n = 5). (I,J) Statistical graphs of GAD67 and GAD65 protein expression (n = 5. GAD67: F = 21.16, $p = 0.0001$. GAD65: F = 20.70, $p = 0.0001$). (K) Schematic diagrams of waveforms obtained by EMG in SCI + Veh, SCI + Chst11, and SCI + Chst11 + EA groups. (L,M) Statistical graphs of EMG signals of the gastrocnemius muscle in the hind limbs of rats in SCI + Veh, SCI + Chst11, and SCI + Chst11 + EA groups (n = 6. Amplitude: F = 36.06, ns: not significant, $p < 0.0001$. Duration: F = 0.8760, $p = 0.4367$). (N,O) mRNA expression of *Chst11* and *Chst3* in the three groups on day 14 after SCI (*Chst11*: n = 5, F = 3.030, $p = 0.0860$. *Chst3*: n = 5–6, F = 1.192, $p = 0.3327$). *$p < 0.05$. Data are expressed as mean ± SEM. (E), (F), (G), (I), (J) and (L–O) were performed using one-way ANOVA, followed by Tukey's post hoc test. Fig. 5A,K were created using Adobe Illustrator 2019 (23.0.3 x64, Adobe Systems Incorporated)

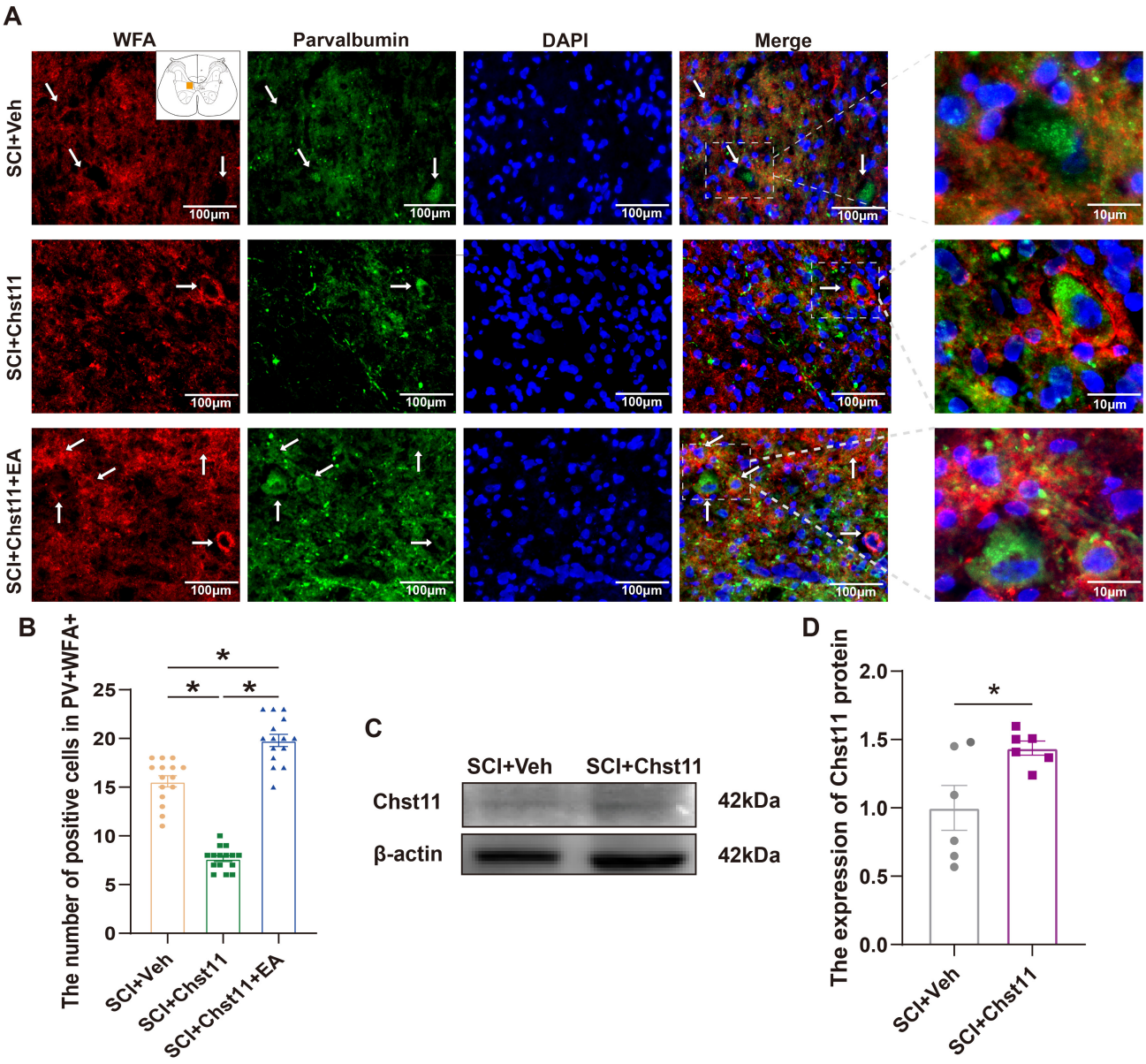

Fig. 6. EA reversed the Chst11-induced reduction in the number of PNN and PV IN positive cells. (A) Representative fluorescence plots of WFA + PV+ in SCI + Veh, SCI + Chst11, and SCI + Chst11 + EA groups at day 14. (Scale bar = 100 μm and 10 μm). White arrows indicate relevant positive staining points. The white box marks the rightmost magnified area. (B) Statistical graph of the number of WFA + PV + positive cells in SCI + Veh, SCI + Chst11, and SCI + Chst11 + EA groups illustrated by IF. Each rat contains 5 sections. Statistical analysis of the data results was performed using one-way ANOVA, followed by Tukey's post hoc test (n = 3, F = 141.3, $p <$ 0.0001). (C) Chst11 protein expression in SCI + Veh and SCI + Chst11 groups on day 14 after SCI. (D) Statistical graph of Chst11 protein expression in SCI + Veh and SCI + Chst11 groups. Statistical analysis of the data results was performed using Student's *t*-test (two-tailed) (n = 6, $p = 0.0297$). *$p < 0.05$. Data are expressed as mean ± SEM. WFA, wisteria floribunda agglutinin; IF, immunofluorescence.

effects analysis also revealed a significant effect of time on BBB scores ($F_{(3,96)} = 1578$, $p < 0.0001$). The SCI + EA group exhibited higher BBB scores on day 14 than on day 7 ($p = 0.0073$). Motor function was significantly improved in rats after EA intervention (Fig. 4A). EMG signal detection results indicated that the amplitude and duration were significantly higher in the SCI + EA group than in the SCI + ShamEA group (Fig. 4B,F,G). EA significantly promoted SCI repair, effectively increased the expression levels of C4S and C6S (Fig. 4C–E), and improved PNN stability (Fig. 4C). The GAD protein expression results were consistent with those of CS (Fig. 4H–J). EA significantly increased CS and GAD expression and promoted SCI repair.

3.5 EA Reverses the Inhibitory Effect Caused by Chst11

When normal rats contained more Chst11 than the normal range, their PNN inhibitory properties were enhanced, and the rate of spinal cord repair was inhibited following SCI. Based on this characterization, we injected the virus overexpressing Chst11 into the spinal cord of rats at the junction of T9 and T10 28 days prior, and it was fully expressed in the T10 segment (Fig. 5A,B). Subsequently, we verified the efficiency of Chst11 overexpression (Fig. 6C,D). To investigate the potential of EA in promoting SCI repair by inhibiting Chst11 and modulating CS and GAD expression, we administered EA with a virus containing Chst11 to rats for 14 days, followed by detection and analysis of T10 spinal cord segments. The results of BBB scores revealed a significant interaction between group (intervention) and time ($F_{(6,60)} = 6.563$, $p < 0.0001$). Analysis of main effects showed that group (intervention) significantly influenced BBB scores ($F_{(2,60)} = 18.53$, $p < 0.0001$). At Day 14, the SCI + Chst11 + EA group scored significantly higher than the SCI + Chst11 group ($p < 0.0001$). The main effects analysis also revealed a significant effect of time on BBB scores ($F_{(3,60)} = 1264$, $p < 0.0001$). The SCI + Chst11 + EA group exhibited higher BBB scores on day 14 than on day 7 ($p = 0.0011$). EA reversed the inhibitory effect of Chst11, and motor function was significantly improved in the SCI + Chst11 + EA group (Fig. 5C). The amplitude of the hindlimb unit EMG was significantly higher in the SCI + Chst11 + EA group than in the SCI + Chst11 group (Fig. 5K–M). C4S and C6S protein expression levels were significantly higher in the SCI + Chst11 + EA group than in the SCI + Chst11 group, and the inhibitory properties of Chst11 were reversed by EA, promoting SCI recovery (Fig. 5D–F). The EA reversed Chst11 inhibition and improved PNN stability (Fig. 5G). GAD67 and 65 also displayed similarities to C4S and C6S protein expression (Fig. 5H–J).

The results of qRT-PCR similarly indicated that EA did not alter the endogenous expression of CS-related synthase genes in rats while promoting SCI recovery, suggesting that its impact on the organism was minimal (Fig. 5N,O). IF results were consistent with those of WB, and EA effectively increased the number of PNN and PV IN after SCI, facilitating SCI repair (Fig. 6A,B). The original western blot data for this study are provided in the **Supplementary Materials-WB**.

4. Discussion

After SCI, the volume and number of individual PNN around motor neurons at the site of injury decrease, and structural and functional remodeling occur [22], which is accompanied by atrophy of inhibitory gamma-aminobutyric acid ergic (GABAergic) interneurons and decreased expression of PV IN [23]. We observed reduced calcium activity of PV IN, as well as CS, and GAD expression levels, in response to PV IN activity and expression in an SCI model [24,25]. In contrast, EA intervention reversed this effect and effectively facilitated SCI repair.

PNN, a densely aggregated form of ECM with a lattice-like network structure and a negative charge, is widely present around many neurons in the spinal cord [26]. It predominantly wraps around the rapidly spiking γ-aminobutyric acidergic PV IN and encircles motor neurons along the spinal cord [27]. The functions of PNN in the nervous system, such as ion buffering, neuroprotection, and neuromaturation, benefit from their structural integrity [28–30]. When the spinal cord is damaged, the structure of the PNN is disrupted, and a reduction in thickness occurs [5], upsetting the balance between plasticity and stability [5]. PNN reduction causes uncontrolled spinal cord sprouting and increased neuronal excitability [31–33], leading to hyperexcitability of spinal cord circuits and maladaptive symptoms, such as neuropathic pain and spasticity [34,35]. Accordingly, the integrity of PNN after SCI is important for the subsequent recovery of spinal cord neurological function, as demonstrated in the previous part of this study and by others [36]. Consequently, excessive disruption of PNN disrupts its reorganization after injury, leading to increased motor deficits [37].

CSPGs are the primary components of PNN [38], and all types of CSPGs are composed of core proteins and a variable number of CS-GAG chains [39,40], whose high negative charge is an essential determinant of PNN functions [41,42]. This is because the high-intensity negative charge carried by CS-GAG can buffer cations generated after oxidative stress or toxic metal ions, thereby conferring neuroprotection to PNN [43–45]. Previous studies have suggested that C4S inhibits axonal growth and suppresses neuronal plasticity, whereas C6S promotes axonal growth and enhances plasticity [10,46,47]. CS-GAG is essential for PNN stability. Excessive degradation of CS-GAG causes excessive plasticity and increases the susceptibility of nerves to neurotoxic stimuli [5]. This study revealed that after SCI, the expression of CS, which represents an essential component of PNN function, decreased, accompanied by downregulation of GAD expression. This suggests that PNN structure was damaged differently after SCI due to the decrease in CS expression caused by the injury, leading to a sudden reduction in the number of PNN that WFA can recognize in the injured area and a similar decrease in the number of PV IN. Simultaneously, the homeostatic balance of neurons, initially maintained by PNN, was disrupted, and the plasticity of neurons was enhanced due to the reduction in PNN. When the damaged area was repaired and CS expression was significantly upregulated, the number of PNN also increased, as did the number and activity of PV IN, indicating that CS has an essential influence on the production and functional expression of PNN and the activity of PV IN. However, in this study, we found that GAD67 protein expression remained unchanged on day 1 post-injury, whereas GAD65

expression significantly increased during this period. As GAD65 and GAD67 are primarily expressed in GABAergic interneurons, the difference in their expression levels stems from the distinct regulatory mechanisms governing different interneuron subtypes. We hypothesized that GAD67 expression may decrease post-injury due to hypoxia and glutamate toxicity compared to GAD65 at the same time point. Conversely, GAD65 remains inactive under normal conditions but rapidly transitions to an active state in response to neurotrauma-induced GABAergic synaptic activity within a short timeframe, thereby increasing its expression levels [48]. The precise mechanisms underlying these differences remain to be explored, and we plan to investigate this phenomenon in subsequent studies.

Following SCI, mechanical trauma induces glial cells, which maintain central nervous system stability, to release toxins and multiple cytokines, endowing them with pathological and reparative properties. SCI activates perivascular cells and astrocytes, causing peripheral fibroblasts and Schwann cells to aggregate at the injury site, thereby forming glial scars and fibrotic scar tissue [49]. Astrocytes are the primary components of glial scar formation. Following SCI, astrocytes become activated, exhibiting hypertrophic changes, synapse growth, and increased expression of glial fibrillary acidic protein, transforming into reactive astrocytes (RA) [50]. Continuous aggregation and overlapping of RAs transform them into scar-forming astrocytes, forming extensive glial scars at the injury site. This inhibits axonal regeneration and limits SCI recovery [51]. Following SCI, disruption of PNN structure and stability leads to extensive deposition of ECM molecules at the injury site, thereby forming fibrotic scar tissue [52]. Concurrently, astrocyte formation interferes with ECM deposition, inhibiting endogenous repair of SCI. The resulting glial and fibrotic scars may impede the transport of CS-GAG to the damaged PNN, thereby hindering PNN repair. Since CS-GAG is a crucial component of the neuroprotective function of PNN, injury sites encapsulated by the glial scar lack the protective effects of a structurally intact PNN, further obstructing SCI repair.

The C4S/C6S ratio in the spinal cord affects PNN function and production. An increase in the C4S/C6S ratio promotes PNN formation during the developmental stage of neurons, suggesting a significant increase in PV IN during the neuronal developmental stage. However, a decrease in the C4S/C6S ratio at the stage of neuronal injury opens up the plasticity of PNN, suggesting that the structure of PNN is disrupted to some extent at the injury site [10]. The lower the C4S/C6S ratio, the more susceptible the mouse brain is to external stimuli that induce epileptic symptoms [53]. The results of this study on rats under different interventions after SCI revealed that a decrease in the C4S/C6S ratio represented the disruption of PNN stability and neuronal plasticity. When SCI was intervened and repaired, the upregulation of the ratio represented the reorganization of PNN structure, and the stabilizing function for maintaining the homeostatic environment of neurons was restored. Since PV IN was encapsulated by PNN, the restoration of PNN caused by the increase in the C4S/C6S ratio in the localized spinal cord after the intervention promoted the formation and expression of PV IN to some extent.

C4ST-1/Chst11 is an enzyme involved in CS sulfation that catalyzes the transfer of the sulfate group from the donor to the carbon-4 position of N-acetylgalactosamine to complete C4S sulfation [4]. Excessive C4S expression increases the inhibitory properties of PNN [54], increases structural stability, and decreases the ability to repair after injury. Transferase enzymes, such as Chst11, have been suggested to be key factors in fine sulfation homeostasis and indirectly influence neural maturation and stabilization of the CNS [8,55]. The damaged spinal cord of zebrafish was repaired more rapidly after Chst11 knockdown, while the presence of Chst11 inhibited the progress of spinal cord repair [9]. In this study, we found that after injecting a virus overexpressing Chst11 into normal rats, the inhibitory properties of the rats were enhanced by localized genetic changes. After preparing the SCI model, the results revealed that rats injected with a virus containing Chst11 did not express sufficient CS-GAG. Combined with the results of previous studies, we suggest that this is due to the inhibitory effect of Chst11, causing a significant reduction in the repair capacity at the site of injury. This phenomenon was alleviated after subsequent EA intervention. This suggests that excessive Chst11 causes deterioration of the neuronal environment and increased inhibition at the injury site. However, EA can alleviate this situation, improve the neuronal external environment at the injury site, and promote injury repair.

In the CNS, especially in the spinal cord, PNN is predominantly wrapped around the fast-spiking PV IN [27], a type of inhibitory γ-aminobutyric acid interneuron, and there is a close relationship between the timing of its maturation and the development of PNN [56]. PV IN prevents small-conductance Ca2+-activated K+ channels (SK channels) activation by buffering spike-mediated calcium influx and enables rapid spike discharge [57–59]. Reduced expression of PV IN and the consequent accumulation of intracellular calcium decrease the rapid spike discharge of PV IN and reduce its inhibitory output and effect [59]. After SCI, PV IN are more susceptible to damage from neurodegeneration, extracellular oxidative stress, and reduced neuronal function because PNN structure is disrupted, and the number of PNN wrapped around PV IN is reduced [44]. This study found a significant decrease in PV IN expression and activity after SCI, confirming this hypothesis. One study has also found that increasing PV IN activity reduces pain caused by nerve damage and promotes nerve repair [59]. In this study, following therapeutic intervention at the injured site of SCI, the structural reorganization of PNN increased the excitability and activity of PV IN, indicating

the importance of PV IN in SCI repair. We found that PV IN follows the SCI repair process and changes accordingly. From the low expression on SCI day 7 to the upregulation on SCI day 14, the overall function of PV IN was constantly repaired and enhanced by the significant increase in GAD expression by EA. The repair process of SCI is the re-expression process of PV IN.

The effect of CS-GAG on PV IN function is also important, as CS deletion reduces the spiking response of PV IN [11]. Maturation of PV IN promotes PNN development and the sulfation pattern of CS-GAG. Thus, the sulfation mode pattern of CS-GAG can promote the maturation of PV IN and maintain cellular function [11]. The stable PNN structure, in which CS-GAG participates, also provides neuroprotection to PV IN.

We chose to use jia-ji acupoints (EX-B2) because they are primarily located on both sides of the spinal column, approximately 1.5 cm away from the spinal cord. There are 17 pairs of acupoints from T1 to L5, all of which are in proximity to the spinal cord. These acupoints can effectively promote recovery in the adjacent spinal cord. In this study, we selected the jia-ji acupoints near T9–T11, which are located at the upper and lower segments of the T10 injury site, and the EA intervention can effectively promote the recovery of SCI, which has been confirmed in our previous studies and clinical data analysis [13,15,21,60]. Due to the proximity of these points to the chest and spinal cord, they can cause several adverse reactions if not handled appropriately. Through our observations and studies, we did not find any adverse reactions to EA in mice and rats, and no cases of death in mice and rats were attributed to EA. In clinical treatment, acupuncture has minor adverse reactions when targeting different diseases and patients; however, these can be avoided by adjusting the patient's position and adequate preparation. Individual adverse effects may vary in degree due to personal differences, but overall, EA or acupuncture remains a safe intervention [61].

Electroacupuncture stimulation of EX-B2, followed by a specific parameter of electrical stimulation, is a traditional acupuncture technique that has been modernized in the context of therapy. EA stimulation of the EX-B2 can regulate the local blood supply and stimulate local nerve excitation, thereby promoting nerve repair at the site of injury. EA can improve the microenvironment of neurons at the SCI site, improve local blood supply, alleviate lower body paraplegia caused by SCI, and promote long-term recovery of neurological function in patients [62]. Previous treatment options for SCI, such as the application of biomaterials [63], stem cell therapy [64], delivery of nanomedicines [65] or ultrasound stimulation [66], and other traditional invasive and novel non-invasive therapies, have been associated with high costs, drug side effects, and high technical requirements. In contrast, EA only requires a cheap stainless-steel needle and an electrical stimulation device with an appropriate frequency for SCI treatment, which is effective and safe. From this perspective, EA has several advantages, including high-cost performance, simplicity of operation, safety, and effectiveness, and is expected to become a new technology for SCI treatment.

Additionally, through BBB scoring and hindlimb EMG testing in this study, we found that EA demonstrated favorable effects on restoring hindlimb motor function in rats with spinal cord injury. Based on changes in BBB scores, we can clearly determine the recovery stage of the rats' hindlimbs. However, since BBB scoring is limited to evaluating hindlimb motor function in rats and cannot be directly applied clinically, existing guidelines or standards should be referenced for a more detailed assessment of patients' limb motor function in actual clinical practice. Although the BBB scoring system cannot be directly applied in clinical practice, it indirectly reflects that EA treatment for SCI encompasses motor function aspects. This finding may further expand the clinical application scenarios for EA.

In this study, we observed that EA significantly enhanced PNN stability after SCI, increased PV IN activity, and promoted CS and GAD expression. Additionally, EA reversed the inhibitory effect of Chst11 and increased the expression levels of PNN and PV IN, thereby maintaining neuronal stability and promoting the recovery of neuronal functions. In summary, EA enhanced the stability of PNN and PV IN by increasing CS-GAG expression, thereby promoting SCI rehabilitation in rats.

In conclusion, the effectiveness and mechanisms of EA must be validated and elucidated; however, this does not prevent EA from being used as a safe and effective means of treating SCI.

5. Conclusion

The mechanism and effects of EA on SCI repair were investigated. The results revealed that EA could regulate the recovery of PNN structure and function via CS-GAG and GAD, improve PV IN activity, and reverse the inhibitory effect of Chst11 to promote SCI rehabilitation in rats.

Abbreviations

BBB, Basso–Beattie–Bresnahan; Chst11, Carbohydrate sulfotransferase 11; C4ST-1, Chondroitin-4-sulfotransferase-1; CNS, Central nervous system; CSPG, Chondroitin sulfate proteoglycan; CS-GAG, Chondroitin sulfate glycosaminoglycan; C4S, Chondroitin 4-sulfation; C6S, Chondroitin 6-sulfation; CS, Chondroitin sulfate; ChABC, Chondroitinase ABC; EA, Electroacupuncture; ECM, Extracellular matrix; GAD65/67, Glutamic acid decarboxylase 65/67; IF, Immunofluorescence; PV IN, Parvalbumin interneuron; PNN, Perineuronal net; PV, Parvalbumin; qRT-PCR, Quantitative Real-Time Polymerase Chain Reaction; SCI, Spinal cord injury; WB,

Western blotting; WFA, Wisteria floribunda lectin; EMG, Electromyography; SD, Sprague-Dawley.

Disclosure

This paper has been posted as a preprint on Research Square with doi: https://doi.org/10.21203/rs.3.rs-3404696/v1, which is available from: https://www.researchsquare.com/article/rs-3404696/v1.

Availability of Data and Materials

The datasets used and analyzed during the current study are available from the corresponding author on reasonable request.

Author Contributions

RM, BC, and RH designed the study; BC, RH, XW, and JZ conducted the research; MS, YC, YH, and DH contributed to obtaining results and data; XY organized results and data and provided preliminary interpretations; BC, RH, MS, YH, and RM performed data analysis; BC and RH drafted the manuscript. YC and XY refined the manuscript structure and content and provided assistance and suggestions regarding the impact factor section. RM and DH provided major constructive feedback during manuscript revisions and finalized the draft. All authors contributed to editorial changes in the manuscript. All authors read and approved the final manuscript. All authors have participated sufficiently in the work and agreed to be accountable for all aspects of the work.

Ethics Approval and Consent to Participate

All animal experiments were conducted in accordance with all relevant animal testing and research ethics regulations and in accordance with the animal protocol approved by the Animal Ethics Committee of Zhejiang University of Chinese Medicine (ZSLL, 2017183). This study was conducted in accordance with the National Institutes of Health Guide for the Care and Use of Laboratory Animals.

Acknowledgment

We sincerely thank the third clinical college of Zhejiang Chinese Medical University, Hangzhou, Zhejiang, China for offering the experimental areas and instruments.

Funding

This study was supported by National Natural Science Foundation of China (No. 82174487 and 82505780). Special project of the Affiliated Hospital of Zhejiang Chinese Medical University (No. 2022FSYYZZ08 and 2022FSYYZY09).

Conflict of Interest

The authors declare no conflict of interest.

Supplementary Material

Supplementary material associated with this article can be found, in the online version, at https://doi.org/10.31083/JIN46448.

References

[1] Wu Y, Chen H, Tan Z, Li D, Liang C. Therapeutic effects of Erbin inhibitor on spinal cord contusion in mice. American Journal of Translational Research. 2019; 11: 2570–2579.

[2] Badhiwala JH, Ahuja CS, Akbar MA, Witiw CD, Nassiri F, Furlan JC, *et al*. Degenerative cervical myelopathy - update and future directions. Nature Reviews. Neurology. 2020; 16: 108–124. https://doi.org/10.1038/s41582-019-0303-0.

[3] Willis A, Pratt JA, Morris BJ. Enzymatic Degradation of Cortical Perineuronal Nets Reverses GABAergic Interneuron Maturation. Molecular Neurobiology. 2022; 59: 2874–2893. https://doi.org/10.1007/s12035-022-02772-z.

[4] Mizumoto S, Mikami T, Yasunaga D, Kobayashi N, Yamauchi H, Miyake A, *et al*. Chondroitin 4-O-sulfotransferase-1 is required for somitic muscle development and motor axon guidance in zebrafish. The Biochemical Journal. 2009; 419: 387–399. https://doi.org/10.1042/BJ20081639.

[5] Sánchez-Ventura J, Lane MA, Udina E. The Role and Modulation of Spinal Perineuronal Nets in the Healthy and Injured Spinal Cord. Frontiers in Cellular Neuroscience. 2022; 16: 893857. https://doi.org/10.3389/fncel.2022.893857.

[6] Habuchi O. Functions of chondroitin/dermatan sulfate containing GalNAc4,6-disulfate. Glycobiology. 2022; 32: 664–678. https://doi.org/10.1093/glycob/cwac030.

[7] Pan H, Xue W, Zhao W, Schachner M. Expression and function of chondroitin 4-sulfate and chondroitin 6-sulfate in human glioma. FASEB Journal: Official Publication of the Federation of American Societies for Experimental Biology. 2020; 34: 2853–2868. https://doi.org/10.1096/fj.201901621RRR.

[8] Klüppel M. The roles of chondroitin-4-sulfotransferase-1 in development and disease. Progress in Molecular Biology and Translational Science. 2010; 93: 113–132. https://doi.org/10.1016/S1877-1173(10)93006-8.

[9] Sahu S, Li R, Loers G, Schachner M. Knockdown of chondroitin-4-sulfotransferase-1, but not of dermatan-4-sulfotransferase-1, accelerates regeneration of zebrafish after spinal cord injury. FASEB Journal: Official Publication of the Federation of American Societies for Experimental Biology. 2019; 33: 2252–2262. https://doi.org/10.1096/fj.201800852RR.

[10] Miyata S, Komatsu Y, Yoshimura Y, Taya C, Kitagawa H. Persistent cortical plasticity by upregulation of chondroitin 6-sulfation. Nature Neuroscience. 2012; 15: 414–422. https://doi.org/10.1038/nn.3023.

[11] Igarashi M, Takeuchi K, Sugiyama S. Roles of CSGalNAcT1, a key enzyme in regulation of CS synthesis, in neuronal regeneration and plasticity. Neurochemistry International. 2018; 119: 77–83. https://doi.org/10.1016/j.neuint.2017.10.001.

[12] Ballon Romero SS, Fuh LJ, Hung SY, Lee YC, Huang YC, Chien SY, *et al*. Electroacupuncture exerts prolonged analgesic and neuroprotective effects in a persistent dental pain model induced by multiple dental pulp injuries: GABAergic interneurons-astrocytes interaction. Frontiers in Immunology. 2023; 14: 1213710. https://doi.org/10.3389/fimmu.2023.1213710.

[13] Ma R, Liu X, Clark J, Williams GM, Doi SA. The Impact of Acupuncture on Neurological Recovery in Spinal Cord Injury: A Systematic Review and Meta-Analysis. Journal of Neurotrauma. 2015; 32: 1943–1957. https://doi.org/10.1089/neu.2014.3866.

[14] Zeng YS, Ding Y, Xu HY, Zeng X, Lai BQ, Li G, *et al*. Electroacupuncture and its combination with adult stem cell transplantation for spinal cord injury treatment: A summary of current laboratory findings and a review of literature. CNS Neuroscience & Therapeutics. 2022; 28: 635–647. https://doi.org/10.1111/cns.13813.

[15] Hu R, Xu H, Jiang Y, Chen Y, He K, Wu L, *et al*. EA Improves the Motor Function in Rats with Spinal Cord Injury by Inhibiting Signal Transduction of Semaphorin3A and Upregulating of the Peripheral Nerve Networks. Neural Plasticity. 2020; 2020: 8859672. https://doi.org/10.1155/2020/8859672.

[16] Hu R, Chen Y, Xu HP, He KL, Sun LZ, Wu L, *et al*. Effect of electroacupuncture at "Jiaji" (EX-B 2) points on the proliferation and differentiation of oligodendrocyte precursor cells in rats with acute spinal cord injury. Zhongguo Zhen Jiu = Chinese Acupuncture & Moxibustion. 2020; 40: 519–525. https://doi.org/10.13703/j.0255-2930.20190326-0008. (In Chinese)

[17] Chau CH, Shum DKY, Li H, Pei J, Lui YY, Wirthlin L, *et al*. Chondroitinase ABC enhances axonal regrowth through Schwann cell-seeded guidance channels after spinal cord injury. FASEB Journal: Official Publication of the Federation of American Societies for Experimental Biology. 2004; 18: 194–196. https://doi.org/10.1096/fj.03-0196fje.

[18] Lee H, McKeon RJ, Bellamkonda RV. Sustained delivery of thermostabilized chABC enhances axonal sprouting and functional recovery after spinal cord injury. Proceedings of the National Academy of Sciences of the United States of America. 2010; 107: 3340–3345. https://doi.org/10.1073/pnas.0905437106.

[19] Basso DM, Beattie MS, Bresnahan JC. A sensitive and reliable locomotor rating scale for open field testing in rats. Journal of Neurotrauma. 1995; 12: 1–21. https://doi.org/10.1089/neu.1995.12.1.

[20] Zhang W, Xiong BR, Zhang LQ, Huang X, Yuan X, Tian YK, *et al*. The Role of the GABAergic System in Diseases of the Central Nervous System. Neuroscience. 2021; 470: 88–99. https://doi.org/10.1016/j.neuroscience.2021.06.037.

[21] Hu R, He K, Chen B, Chen Y, Zhang J, Wu X, *et al*. Electroacupuncture promotes the repair of the damaged spinal cord in mice by mediating neurocan-perineuronal net. CNS Neuroscience & Therapeutics. 2024; 30: e14468. https://doi.org/10.1111/cns.14468.

[22] Lipachev N, Arnst N, Melnikova A, Jäälinoja H, Kochneva A, Zhigalov A, *et al*. Quantitative changes in perineuronal nets in development and posttraumatic condition. Journal of Molecular Histology. 2019; 50: 203–216. https://doi.org/10.1007/s10735-019-09818-y.

[23] Favuzzi E, Marques-Smith A, Deogracias R, Winterflood CM, Sánchez-Aguilera A, Mantoan L, *et al*. Activity-Dependent Gating of Parvalbumin Interneuron Function by the Perineuronal Net Protein Brevican. Neuron. 2017; 95: 639–655.e10. https://doi.org/10.1016/j.neuron.2017.06.028.

[24] Yang S, Gigout S, Molinaro A, Naito-Matsui Y, Hilton S, Foscarin S, *et al*. Chondroitin 6-sulphate is required for neuroplasticity and memory in ageing. Molecular Psychiatry. 2021; 26: 5658–5668. https://doi.org/10.1038/s41380-021-01208-9.

[25] Zeng C, Lei D, Lu Y, Huang Q, Wu Y, Yang S, *et al*. Parvalbumin in the metabolic pathway of glutamate and γ-aminobutyric acid: Influence on expression of GAD65 and GAD67. Archives of Biochemistry and Biophysics. 2023; 734: 109499. https://doi.org/10.1016/j.abb.2022.109499.

[26] Li X, Wu X, Lu T, Kuang C, Si Y, Zheng W, *et al*. Perineuronal Nets in the CNS: Architects of Memory and Potential Therapeutic Target in Neuropsychiatric Disorders. International Journal of Molecular Sciences. 2024; 25: 3412. https://doi.org/10.3390/ijms25063412.

[27] van 't Spijker HM, Kwok JCF. A Sweet Talk: The Molecular Systems of Perineuronal Nets in Controlling Neuronal Communication. Frontiers in Integrative Neuroscience. 2017; 11: 33. https://doi.org/10.3389/fnint.2017.00033.

[28] Bozzelli PL, Alaiyed S, Kim E, Villapol S, Conant K. Proteolytic Remodeling of Perineuronal Nets: Effects on Synaptic Plasticity and Neuronal Population Dynamics. Neural Plasticity. 2018; 2018: 5735789. https://doi.org/10.1155/2018/5735789.

[29] Fawcett JW, Oohashi T, Pizzorusso T. The roles of perineuronal nets and the perinodal extracellular matrix in neuronal function. Nature Reviews. Neuroscience. 2019; 20: 451–465. https://doi.org/10.1038/s41583-019-0196-3.

[30] Bosiacki M, Gąssowska-Dobrowolska M, Kojder K, Fabiańska M, Jeżewski D, Gutowska I, *et al*. Perineuronal Nets and Their Role in Synaptic Homeostasis. International Journal of Molecular Sciences. 2019; 20: 4108. https://doi.org/10.3390/ijms20174108.

[31] Sánchez-Ventura J, Giménez-Llort L, Penas C, Udina E. Voluntary wheel running preserves lumbar perineuronal nets, enhances motor functions and prevents hyperreflexia after spinal cord injury. Experimental Neurology. 2021; 336: 113533. https://doi.org/10.1016/j.expneurol.2020.113533.

[32] Oudega M, Perez MA. Corticospinal reorganization after spinal cord injury. The Journal of Physiology. 2012; 590: 3647–3663. https://doi.org/10.1113/jphysiol.2012.233189.

[33] Hayani H, Song I, Dityatev A. Increased Excitability and Reduced Excitatory Synaptic Input Into Fast-Spiking CA2 Interneurons After Enzymatic Attenuation of Extracellular Matrix. Frontiers in Cellular Neuroscience. 2018; 12: 149. https://doi.org/10.3389/fncel.2018.00149.

[34] Mòdol L, Cobianchi S, Navarro X. Prevention of NKCC1 phosphorylation avoids downregulation of KCC2 in central sensory pathways and reduces neuropathic pain after peripheral nerve injury. Pain. 2014; 155: 1577–1590. https://doi.org/10.1016/j.pain.2014.05.004.

[35] Hu X, Du L, Liu S, Lan Z, Zang K, Feng J, *et al*. A TRPV4-dependent neuroimmune axis in the spinal cord promotes neuropathic pain. The Journal of Clinical Investigation. 2023; 133: e161507. https://doi.org/10.1172/JCI161507.

[36] Sánchez-Ventura J, Canal C, Hidalgo J, Penas C, Navarro X, Torres-Espin A, *et al*. Aberrant perineuronal nets alter spinal circuits, impair motor function, and increase plasticity. Experimental Neurology. 2022; 358: 114220. https://doi.org/10.1016/j.expneurol.2022.114220.

[37] Orlando C, Raineteau O. Integrity of cortical perineuronal nets influences corticospinal tract plasticity after spinal cord injury. Brain Structure & Function. 2015; 220: 1077–1091. https://doi.org/10.1007/s00429-013-0701-9.

[38] Milton AJ, Kwok JCF, McClellan J, Randall SG, Lathia JD, Warren PM, *et al*. Recovery of Forearm and Fine Digit Function After Chronic Spinal Cord Injury by Simultaneous Blockade of Inhibitory Matrix Chondroitin Sulfate Proteoglycan Production and the Receptor PTPσ. Journal of Neurotrauma. 2023; 40: 2500–2521. https://doi.org/10.1089/neu.2023.0117.

[39] Dauth S, Grevesse T, Pantazopoulos H, Campbell PH, Maoz BM, Berretta S, *et al*. Extracellular matrix protein expression is brain region dependent. The Journal of Comparative Neurology. 2016; 524: 1309–1336. https://doi.org/10.1002/cne.23965.

[40] Miyata S, Kitagawa H. Formation and remodeling of the brain extracellular matrix in neural plasticity: Roles of chondroitin sulfate and hyaluronan. Biochimica et Biophysica Acta. General Subjects. 2017; 1861: 2420–2434. https://doi.org/10.1016/j.bbagen.2017.06.010.

[41] Brückner G, Brauer K, Härtig W, Wolff JR, Rickmann MJ, Derouiche A, *et al*. Perineuronal nets provide a polyanionic, glia-associated form of microenvironment around certain neu-

rons in many parts of the rat brain. Glia. 1993; 8: 183–200. https://doi.org/10.1002/glia.440080306.

[42] Scarlett JM, Hu SJ, Alonge KM. The "Loss" of Perineuronal Nets in Alzheimer's Disease: Missing or Hiding in Plain Sight? Frontiers in Integrative Neuroscience. 2022; 16: 896400. https://doi.org/10.3389/fnint.2022.896400.

[43] Morawski M, Brückner G, Jäger C, Seeger G, Arendt T. Neurons associated with aggrecan-based perineuronal nets are protected against tau pathology in subcortical regions in Alzheimer's disease. Neuroscience. 2010; 169: 1347–1363. https://doi.org/10.1016/j.neuroscience.2010.05.022.

[44] Suttkus A, Rohn S, Weigel S, Glöckner P, Arendt T, Morawski M. Aggrecan, link protein and tenascin-R are essential components of the perineuronal net to protect neurons against iron-induced oxidative stress. Cell Death & Disease. 2014; 5: e1119. https://doi.org/10.1038/cddis.2014.25.

[45] Reichelt AC, Hare DJ, Bussey TJ, Saksida LM. Perineuronal Nets: Plasticity, Protection, and Therapeutic Potential. Trends in Neurosciences. 2019; 42: 458–470. https://doi.org/10.1016/j.tins.2019.04.003.

[46] Sakamoto K, Ozaki T, Kadomatsu K. Axonal Regeneration by Glycosaminoglycan. Frontiers in Cell and Developmental Biology. 2021; 9: 702179. https://doi.org/10.3389/fcell.2021.702179.

[47] Clifford T, Finkel Z, Rodriguez B, Joseph A, Cai L. Current Advancements in Spinal Cord Injury Research-Glial Scar Formation and Neural Regeneration. Cells. 2023; 12: 853. https://doi.org/10.3390/cells12060853.

[48] Lee SE, Lee Y, Lee GH. The regulation of glutamic acid decarboxylases in GABA neurotransmission in the brain. Archives of Pharmacal Research. 2019; 42: 1031–1039. https://doi.org/10.1007/s12272-019-01196-z.

[49] Orr MB, Gensel JC. Spinal Cord Injury Scarring and Inflammation: Therapies Targeting Glial and Inflammatory Responses. Neurotherapeutics: the Journal of the American Society for Experimental NeuroTherapeutics. 2018; 15: 541–553. https://doi.org/10.1007/s13311-018-0631-6.

[50] Hasel P, Liddelow SA. Astrocytes. Current Biology: CB. 2021; 31: R326–R327. https://doi.org/10.1016/j.cub.2021.01.056.

[51] Tamaru T, Kobayakawa K, Saiwai H, Konno D, Kijima K, Yoshizaki S, *et al*. Glial scar survives until the chronic phase by recruiting scar-forming astrocytes after spinal cord injury. Experimental Neurology. 2023; 359: 114264. https://doi.org/10.1016/j.expneurol.2022.114264.

[52] O'Shea TM, Burda JE, Sofroniew MV. Cell biology of spinal cord injury and repair. The Journal of Clinical Investigation. 2017; 127: 3259–3270. https://doi.org/10.1172/JCI90608.

[53] Yutsudo N, Kitagawa H. Involvement of chondroitin 6-sulfation in temporal lobe epilepsy. Experimental Neurology. 2015; 274: 126–133. https://doi.org/10.1016/j.expneurol.2015.07.009.

[54] Huang H, Joffrin AM, Zhao Y, Miller GM, Zhang GC, Oka Y, *et al*. Chondroitin 4-*O*-sulfation regulates hippocampal perineuronal nets and social memory. Proceedings of the National Academy of Sciences of the United States of America. 2023; 120: e2301312120. https://doi.org/10.1073/pnas.2301312120.

[55] Shen Q, Guo Y, Wang K, Zhang C, Ma Y. A Review of Chondroitin Sulfate's Preparation, Properties, Functions, and Applications. Molecules (Basel, Switzerland). 2023; 28: 7093. https://doi.org/10.3390/molecules28207093.

[56] Lépine M, Douceau S, Devienne G, Prunotto P, Lenoir S, Regnauld C, *et al*. Parvalbumin interneuron-derived tissue-type plasminogen activator shapes perineuronal net structure. BMC Biology. 2022; 20: 218. https://doi.org/10.1186/s12915-022-01419-8.

[57] Franconville R, Revet G, Astorga G, Schwaller B, Llano I. Somatic calcium level reports integrated spiking activity of cerebellar interneurons in vitro and in vivo. Journal of Neurophysiology. 2011; 106: 1793–1805. https://doi.org/10.1152/jn.00133.2011.

[58] Eggermann E, Jonas P. How the 'slow' Ca(2+) buffer parvalbumin affects transmitter release in nanodomain-coupling regimes. Nature Neuroscience. 2011; 15: 20–22. https://doi.org/10.1038/nn.3002.

[59] Petitjean H, Pawlowski SA, Fraine SL, Sharif B, Hamad D, Fatima T, *et al*. Dorsal Horn Parvalbumin Neurons Are Gate-Keepers of Touch-Evoked Pain after Nerve Injury. Cell Reports. 2015; 13: 1246–1257. https://doi.org/10.1016/j.celrep.2015.09.080.

[60] Chen Y, Wu L, Shi M, Zeng D, Hu R, Wu X, *et al*. Electroacupuncture Inhibits NLRP3 Activation by Regulating CMPK2 After Spinal Cord Injury. Frontiers in Immunology. 2022; 13: 788556. https://doi.org/10.3389/fimmu.2022.788556.

[61] Xu M, Yang C, Nian T, Tian C, Zhou L, Wu Y, *et al*. Adverse effects associated with acupuncture therapies: An evidence mapping from 535 systematic reviews. Chinese Medicine. 2023; 18: 38. https://doi.org/10.1186/s13020-023-00743-7.

[62] Xiao X, Deng Q, Zeng X, Lai BQ, Ma YH, Li G, *et al*. Transcription Profiling of a Revealed the Potential Molecular Mechanism of Governor Vessel Electroacupuncture for Spinal Cord Injury in Rats. Neurospine. 2022; 19: 757–769. https://doi.org/10.14245/ns.2244452.226.

[63] Wu W, Jia S, Xu H, Gao Z, Wang Z, Lu B, *et al*. Supramolecular Hydrogel Microspheres of Platelet-Derived Growth Factor Mimetic Peptide Promote Recovery from Spinal Cord Injury. ACS Nano. 2023; 17: 3818–3837. https://doi.org/10.1021/acsnano.2c12017.

[64] Xia Y, Zhu J, Yang R, Wang H, Li Y, Fu C. Mesenchymal stem cells in the treatment of spinal cord injury: Mechanisms, current advances and future challenges. Frontiers in Immunology. 2023; 14: 1141601. https://doi.org/10.3389/fimmu.2023.1141601.

[65] Zuo Y, Ye J, Cai W, Guo B, Chen X, Lin L, *et al*. Controlled delivery of a neurotransmitter-agonist conjugate for functional recovery after severe spinal cord injury. Nature Nanotechnology. 2023; 18: 1230–1240. https://doi.org/10.1038/s41565-023-01416-0.

[66] Hong YR, Lee EH, Park KS, Han M, Kim KT, Park J. Ultrasound stimulation improves inflammatory resolution, neuroprotection, and functional recovery after spinal cord injury. Scientific Reports. 2022; 12: 3636. https://doi.org/10.1038/s41598-022-07114-6.